Spin-Selective Transport of Electrons in DNA Double Helix

Ai-Min Guo and Qing-feng Sun*

Institute of Physics, Chinese Academy of Sciences, Beijing 100190, China

(Received 18 January 2012; revised manuscript received 1 April 2012; published 22 May 2012)

The experiment that the high spin selectivity and the length-dependent spin polarization are observed in double-stranded DNA [Science **331**, 894 (2011)], is elucidated by considering the combination of the spin-orbit coupling, the environment-induced dephasing, and the helical symmetry. We show that the spin polarization in double-stranded DNA is significant even in the case of weak spin-orbit coupling, while no spin polarization appears in single-stranded DNA. Furthermore, the underlying physical mechanism and the parameter dependence of the spin polarization are studied.

DOI: 10.1103/PhysRevLett.108.218102 PACS numbers: 87.14.gk, 72.25.−b, 85.75.−d, 87.15.Pc

Molecular spintronics, by combining molecular electronics with spintronics to manipulate the transport of electron spins in organic molecular systems, is regarded as one of the most promising research fields and is now attracting extensive interest [1–4], owing to the long spin relaxation time and the flexibility of organic materials. Unconventional magnetic properties of molecular systems reported in organic spin valves and magnetic tunnel junctions, are attributed to the hybrid states in the organic-magnetic interfaces [5–9] and to single-molecule magnet [4]. Organic molecules would not be suitable candidates for spin-selective transport because of their nonmagnetic properties and weak spin-orbit coupling (SOC) [10].

However, very recently, Göhler *et al.* reported the spin selectivity of photoelectron transmission through self-assembled monolayers of double-stranded DNA (dsDNA) deposited on gold substrate [11]. They found that well-organized monolayers of the dsDNA act as very efficient spin filters with high spin polarization at room temperature for long dsDNA, irrespective of the polarization of the incident light. The spin filtration efficiency increases with increasing length of the dsDNA and contrarily no spin polarization could be observed for single-stranded DNA (ssDNA). These results were further substantiated by direct charge transport measurements of single dsDNA connected between two leads [12]. Although several theoretical models were put forward to investigate the spin-selective properties of DNA molecule based on single helical chain-induced Rashba SOC [13,14], the models neglect the double helix feature of the dsDNA and are somewhat inconsistent with the experimental result that the ssDNA could not be a spin filter. Until now, the underlying physical mechanism remains unclear for high spin selectivity observed in the dsDNA [15,16].

In this Letter, a model Hamiltonian, including the small environment-induced dephasing, the weak SOC, and the helical symmetry, is proposed to investigate the quantum spin transport through the ssDNA and dsDNA connected to nonmagnetic leads. We interpret the experimental results that the electrons transmitted through the dsDNA exhibit high spin polarization, the spin filtration efficiency will be enhanced by increasing the DNA length, and no spin polarization appears for the ssDNA. The physical mechanism arises from the combination of the dephasing, the SOC, and the helical symmetry. No spin polarization could be observed if any aforementioned factor is absent. In addition, the high spin polarization can be observed in a very wide range of the parameters.

The charge transport through the dsDNA, illustrated in Fig. 1, can be simulated by the Hamiltonian:

$$\mathcal{H} = \mathcal{H}_{\mathrm{DNA}} + \mathcal{H}_{\mathrm{lead}} + \mathcal{H}_{c} + \mathcal{H}_{\mathrm{so}} + \mathcal{H}_{d}. \quad (1)$$

Here, $\mathcal{H}_{\mathrm{DNA}} = \sum_{n=1}^{N}[\sum_{j=1}^{2}(\varepsilon_{jn}c_{jn}^{\dagger}c_{jn} + t_{jn}c_{jn}^{\dagger}c_{jn+1}) + \lambda_{n}c_{1n}^{\dagger}c_{2n} + \mathrm{H.c.}]$ is the Hamiltonian of usual two-leg ladder model including the spin degree of freedom [17], with

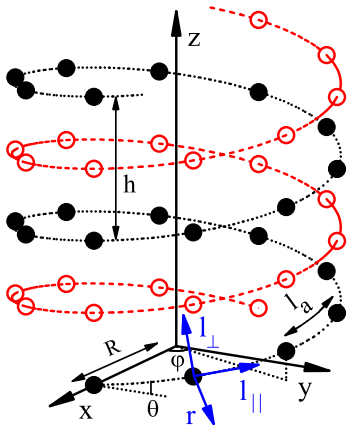

FIG. 1 (color online). Schematic view of the dsDNA with radius R, pitch h, helix angle θ, and arc length l_a. The circles represent the nucleobases, where the full ones assemble one helical chain and the open ones form the other helical chain. The arc length satisfies $l_a\cos\theta = R\Delta\varphi$ and $l_a\sin\theta = \Delta h$, with $\Delta\varphi$ and Δh being the twist angle and the stacking distance between neighboring base-pairs, respectively. We set $\Delta h = 0.34$ nm, $\Delta\varphi = \frac{\pi}{5}$, and $h = 3.4$ nm, which are typical values of B-form DNA. Other parameters are: $R = 0.7$ nm, $\theta \approx 0.66$ rad, and $l_a \approx 0.56$ nm.

 © 2012 American Physical Society

N the DNA length, $c^{\dagger}_{jn} = (c^{\dagger}_{jn\uparrow}, c^{\dagger}_{jn\downarrow})$ the creation operator of the spinor at the nth site of the jth chain of the dsDNA, ε_{jn} the on-site energy, t_{jn} the intrachain hopping integral, and λ_n the interchain hybridization interaction. $\mathcal{H}_{\text{lead}} + \mathcal{H}_c = \sum_{k,\beta(\beta=L,R)}[\varepsilon_{\beta k} a^{\dagger}_{\beta k} a_{\beta k} + t_{\beta} a^{\dagger}_{\beta k}(c_{1n_\beta} + c_{2n_\beta}) + \text{H.c.}]$ describe the left and right nonmagnetic leads and the coupling between the leads and the dsDNA, with $n_L = 1$ and $n_R = N$. $\mathcal{H}_{\text{so}}$ and $\mathcal{H}_d$ are, respectively, the Hamiltonians of the SOC term and the dephasing term, which will be discussed in the following.

When a charge is moving under an electrostatic potential V, an SOC arises $\mathcal{H}_{\text{so}} = \frac{\hbar}{4m^2c^2}\nabla V \cdot (\hat{\sigma} \times \hat{\vec{p}})$, with the electron mass m, the speed of light c, the Pauli matrices $\hat{\sigma} = (\sigma_x, \sigma_y, \sigma_z)$, and the momentum operator $\hat{\vec{p}}$. For the dsDNA which is conductor or semiconductor, the differences of the potential are usually bigger along the radial direction $\hat{r}$ than that along the helix axis (z axis in Fig. 1) [18]. On the other hand, since the differences of V are especially large between the interior and the exterior of the dsDNA, dV/dr is very large at the boundary $r = R$ with R the radius [19]. Hence, it is reasonable to consider the $\hat{r}$ component of V only and the SOC can be simplified in the cylindrical coordinate system $\mathcal{H}_{\text{so}} = -\frac{\alpha}{\hbar}\hat{\sigma} \cdot (\hat{r} \times \hat{\vec{p}})$ with $\alpha \equiv \frac{\hbar^2}{4m^2c^2}\frac{d}{dr}V(r)$. Considering a charge propagating in one helical chain of the dsDNA (e.g., the dotted line in Fig. 1), the momentum $\hat{\vec{p}} = \hat{p}_{\parallel}\hat{l}_{\parallel}$ with $\hat{l}_{\parallel}$ the unit vector along the helical chain direction. Thus $\mathcal{H}_{\text{so}}$ is reduced to $\mathcal{H}_{\text{so}} = -\frac{\alpha}{2\hbar}[\sigma_{\perp}\hat{p}_{\parallel} + \hat{p}_{\parallel}\sigma_{\perp}]$, where $\sigma_{\perp}(\varphi) = \sigma_x \sin\varphi \sin\theta - \sigma_y \cos\varphi \sin\theta + \sigma_z \cos\theta$ with θ the helix angle and φ the cylindrical coordinate. Since the dsDNA consists of two helical chains, the total SOC is $\mathcal{H}_{\text{so}} = -\frac{\alpha}{2\hbar} \times \sum_{j=1}^{2}[\sigma_{\perp}^{(j)}\hat{p}_{\parallel}^{(j)} + \hat{p}_{\parallel}^{(j)}\sigma_{\perp}^{(j)}]$ with $\sigma_{\perp}^{(1)} = \sigma_{\perp}(\varphi)$ and $\sigma_{\perp}^{(2)} = \sigma_{\perp}(\varphi + \pi)$. The interchain SOC has been neglected because it is very small due to the potential symmetry. By using the second quantization [20], $\mathcal{H}_{\text{so}}$ can be written as

$$\mathcal{H}_{\text{so}} = \sum_{j,n} i t_{\text{so}} c^{\dagger}_{jn}[\sigma_n^{(j)} + \sigma_{n+1}^{(j)}]c_{jn+1} + \text{H.c.}, \qquad (2)$$

where $t_{\text{so}} = -\frac{\alpha}{4l_a}$, $\sigma_{n+1}^{(1)} = \sigma_{\perp}(n\Delta\varphi)$, and $\sigma_{n+1}^{(2)} = \sigma_{\perp}(n\Delta\varphi + \pi)$. l_a and $\Delta\varphi$ are, respectively, the arc length and the twist angle between successive base-pairs.

On the other hand, a charge transmitting through the dsDNA will experience inelastic scattering from the phonons due to the fluctuation of each nucleobase around its equilibrium position and other inelastic collisions with the absorbed counterions in the dsDNA due to the negatively charged sugar-phosphate backbones [21]. Such inelastic scattering will give rise to the lose of the phase and spin memory of the charge. Actually, other previous works have clearly indicated the presence of the phase-breaking processes in the DNA molecule [22,23]. To simulate these processes, Büttiker's virtual lead is introduced by connecting to each nucleobase [24,25], with the Hamiltonian of the dephasing term being

$$\mathcal{H}_d = \sum_{j,n,k}(\varepsilon_{jnk} a^{\dagger}_{jnk} a_{jnk} + t_d a^{\dagger}_{jnk} c_{jn} + \text{H.c.}). \qquad (3)$$

$a^{\dagger}_{jnk} = (a^{\dagger}_{jnk\uparrow}, a^{\dagger}_{jnk\downarrow})$ is the creation operator of the virtual lead and t_d is the coupling between the nucleobase and the virtual lead.

Let us demonstrate analytically that the ssDNA could not behave as a spin filter. In continuous real-space spectrum, the Hamiltonian of the ssDNA containing the SOC term is written as $\mathcal{H}_{ss} = \frac{\hat{p}_{\parallel}^2}{2m} - \frac{\alpha}{2\hbar}[\sigma_{\perp}\hat{p}_{\parallel} + \hat{p}_{\parallel}\sigma_{\perp}] + V(l)$ with $V(l)$ the potential energy of the helical chain. By taking a unitary transformation with the operator $U(l) = e^{(im\alpha/\hbar^2)\int_l \sigma_{\perp} dl}$, [26] $\mathcal{H}_{ss}$ is transformed into $\mathcal{H}'_{ss} = U^{\dagger}\mathcal{H}_{ss}U = \frac{\hat{p}_{\parallel}^2}{2m} - \frac{m\alpha^2}{2\hbar^2} + V(l)$, which is independent of spin. Therefore, no spin polarization could be observed in the ssDNA, regardless of the SOC term, the existence of the dephasing, and other model parameters. This result can be obtained also by using the discrete Hamiltonians of Eqs. (1) and (2). Similarly, we can also verify that any kind of SOC could not give rise to spin polarization in the ssDNA. However, for the dsDNA, the charges can transport not only along the helical chain direction, but also within the base-pairs. In this situation, the Hamiltonian cannot be transformed into a spin-independent one, then the results will present a fundamental distinction.

According to the Landauer-Büttiker (LB) formula, the current in the qth lead (real or virtual) with spin s can be written as [27]: $I_{qs} = (e^2/h)\sum_{m,s'} T_{qs,ms'}(V_m - V_q)$, where V_q is the voltage in the qth lead and $T_{qs,ms'} = \text{Tr}[\mathbf{\Gamma}_{qs}\mathbf{G}^r\mathbf{\Gamma}_{ms'}\mathbf{G}^a]$ is the transmission coefficient from the mth lead with spin s' to the qth lead with spin s. The Green function $\mathbf{G}^r = [\mathbf{G}^a]^{\dagger} = [E\mathbf{I} - \mathbf{H}_{\text{DNA}} - \mathbf{H}_{\text{so}} - \sum_{qs}\mathbf{\Sigma}^r_{qs}]^{-1}$ and $\mathbf{\Gamma}_{qs} = i[\mathbf{\Sigma}^r_{qs} - \mathbf{\Sigma}^a_{qs}]$, with E the incident electron energy (or the Fermi energy). $\mathbf{\Sigma}^r_{qs}$ is the retarded self-energy due to the coupling to the qth lead. For the real left/right lead, $\mathbf{\Sigma}_{L/Rs} = -i\Gamma_{L/R}/2 = -i\pi\rho_{L/R}t^2_{L/R}$; while for the virtual leads, $\mathbf{\Sigma}^r_{qs} = -i\Gamma_d/2 = -i\pi\rho_d t_d^2$, with the dephasing parameter Γ_d and $\rho_{L/R/d}$ being the density of states of the leads. Since the net currents through the virtual leads are zero, their voltages can be calculated from the LB formula by applying an external bias V_b between the left and right leads with $V_L = V_b$ and $V_R = 0$. Finally, the conductances for spin-up ($G_{\uparrow}$) and spin-down ($G_{\downarrow}$) electrons can be obtained $G_s = (e^2/h)\sum_{m,s'} T_{Rs,ms'}V_m/V_b$, and the spin polarization is $P_s = (G_{\uparrow} - G_{\downarrow})/(G_{\uparrow} + G_{\downarrow})$.

For the dsDNA, ε_{jn} is set to $\varepsilon_{1n} = 0$ and $\varepsilon_{2n} = 0.3$, t_{jn} is taken as $t_{1n} = 0.12$ and $t_{2n} = -0.1$, and $\lambda_n = -0.3$. All these parameters are extracted from first-principles calculations [28–31] and the unit is eV. The helix angle and the twist angle are set to $\theta \approx 0.66$ rad and $\Delta\varphi = \frac{\pi}{5}$,

respectively. The SOC is estimated to $t_{so} = 0.01$, which is an order of magnitude smaller than the intrachain hopping integral. For the real leads, the parameters $\Gamma_L = \Gamma_R = 1$ are fixed. For the virtual leads, the dephasing strength is small with $\Gamma_d = 0.005$, at which the phase coherence length is about $L_\phi = 14$ [24]. The values of all above-mentioned parameters will be used throughout the Letter except for specific indication in the figure. In fact, the high spin polarization can hold well in a very wide range of the parameters (see below).

Figure 2(a) shows the conductances $G_{\uparrow/\downarrow}$ and the corresponding spin polarization P_s. One notices two transmission bands—the highest occupied molecular orbital (HOMO) and the lowest unoccupied molecular orbital (LUMO)—in the energy spectrum, where several transmission peaks are found for both spin-up and spin-down electrons (holes) due to the coherence of the system. For the HOMO band, $G_\uparrow$ and $G_\downarrow$ are almost identical, while for the LUMO band, $G_\uparrow$ and $G_\downarrow$ are very different. A bell-shaped configuration is observed in the curve of P_s vs energy E, where the spin polarization of the dsDNA at $N = 30$ can achieve 0.44, which is comparable with the experimental results [11].

To explore the physical scenario to high spin polarization observed in the dsDNA, Figs. 2(b) and 2(c) plot the conductance $G_\uparrow$ and P_s in the absence of the dephasing ($\Gamma_d = 0$) and of the helical symmetry ($\theta = \frac{\pi}{2}$), respectively. It clearly appears that the spin polarization vanishes when $\Gamma_d = 0$ or $\theta = \frac{\pi}{2}$, although the conductance is very robust in both cases. When $\Gamma_d = 0$, the dsDNA decouples with the virtual leads and the charge transport through the dsDNA is completely coherent. In this case, the SOC cannot generate any spin polarization due to the time-reversal symmetry, the helical symmetry, and the phase-locking effect [32]. A small dephasing is necessary for the existence of the spin polarization. Indeed, it is reasonable to assume a small Γ_d because the dephasing occurs inevitably in the experiment. On the other hand, the spin polarization strongly depends on the DNA helix. If there is no helix ($\theta = \frac{\pi}{2}$), no spin polarization could be observed ($P_s = 0$). If the right-handed helical dsDNA is transformed into the left-handed one (Z-form DNA) with $\theta \to \pi - \theta$, $P_s(\pi - \theta) = -P_s(\theta)$ exactly.

We then focus on the spin polarization P_s and the averaged one $\langle P_s \rangle$, where $\langle P_s \rangle \equiv (\langle G_\uparrow \rangle - \langle G_\downarrow \rangle)/(\langle G_\uparrow \rangle + \langle G_\downarrow \rangle)$ with $\langle G_s \rangle$ averaged over the LUMO band. Figs. 3(a) and 3(b) show P_s at a fixed energy E and $\langle P_s \rangle$ vs length N, respectively, for several values of the dephasing parameter. One notices that P_s and $\langle P_s \rangle$ are enhanced by increasing N at first and then saturate or slightly decline after a critical length N_c. With increasing Γ_d, N_c shrinks monotonically [Fig. 3(d)]. The behavior of N_c vs Γ_d can be fitted well by a simple function $N_c \propto \Gamma_d^{-1}$. N_c is about 3 times longer than the phase coherence length L_ϕ, implying that high P_s can be observed even if the noncoherent charge transport mechanism dominates. For relatively large Γ_d (diamond and triangle symbols), P_s and $\langle P_s \rangle$ increase faster in the beginning and saturate at shorter length with smaller values because the device is more open. While for smaller Γ_d, P_s and $\langle P_s \rangle$ increase slower with increasing N in a wider range of N and have larger saturation values. Let us see $\Gamma_d = 0.0004$ for instance (circle symbols). P_s and $\langle P_s \rangle$ will keep rising even for $N > 100$, and $P_s = 0.42$ at $N = 40$ and $P_s = 0.55$ at $N = 80$. These results are quantitatively consistent with the experiment [11]. In fact, the dephasing has two effects: (i) it promotes the openness of the two-terminal device and produces the spin polarization [32]; (ii) it makes the charge

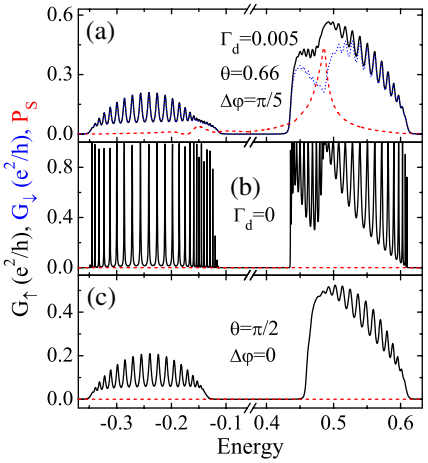

FIG. 2 (color online). (a) Energy dependence of conductance $G_\uparrow$ (solid line), $G_\downarrow$ (dotted line), and spin polarization P_s (dashed line) for realistic situation. (b) and (c) show $G_\uparrow$ and P_s in the absence of the dephasing and of the helical symmetry, respectively. Here, $N = 30$.

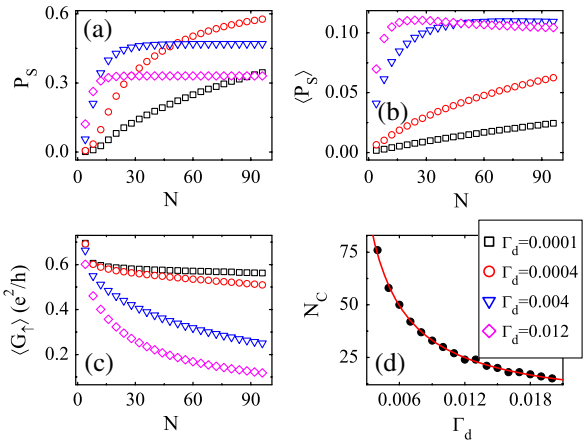

FIG. 3 (color online). Length dependence (a) of P_s at $E = 0.486$, (b) of $\langle P_s \rangle$, and (c) of $\langle G_\uparrow \rangle$ for different values of the dephasing parameter. (d) The critical length N_c vs Γ_d. Here N_c is extracted from the curve of $\langle P_s \rangle$-N and the solid line is the fitting curve with $N_c \propto \Gamma_d^{-1}$. The legends in (d) are for panels (a), (b), and (c).

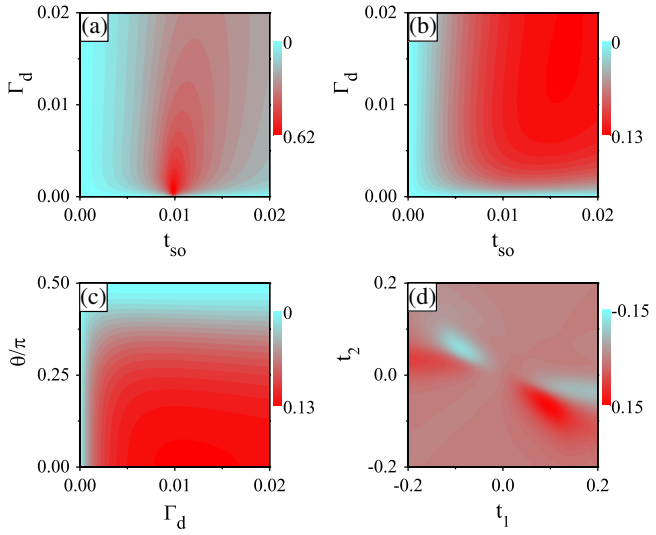

FIG. 4 (color online). (a) P_s vs the SOC t_{so} and the dephasing Γ_d at $E = 0.486$ with $N = 80$. (b), (c), and (d) show $\langle P_s \rangle$ with $N = 30$ as functions of t_{so} and Γ_d, of Γ_d and $\frac{\theta}{\pi}$, and of t_1 and t_2, respectively.

lose its phase and spin memory and then P_s is decreased by further increasing Γ_d. Accordingly, for large Γ_d with the phase coherence length being several base-pairs, P_s will be quite small. $P_s < 0.05$ for $\Gamma_d = 0.5$ and $P_s \to 0$ if $\Gamma_d \to \infty$. Because of the interplay between the above two effects, a small Γ_d, ranging from 0.0002 to 0.01, is optimal for large P_s. Notice that the optimal range of Γ_d is very wide. In addition, Fig. 3(c) shows the averaged conductance $\langle G_\uparrow \rangle$ vs N. $\langle G_\uparrow \rangle$ is declined by increasing N or Γ_d, because large N or Γ_d will enhance the scattering. However, $\langle G_\uparrow \rangle$ remains quite large for $N = 100$ and $\Gamma_d = 0.012$, because of the noncoherent charge transport mechanism [23]. Therefore, the dsDNA is a well spin filter due to the large P_s and $\langle G_\uparrow \rangle$.

Let us further study the spin polarization by varying other model parameters. Figures 4(a) and 4(b) show P_s at $E = 0.486$ with $N = 80$ and $\langle P_s \rangle$ with $N = 30$, respectively, as functions of the SOC t_{so} and the dephasing strength Γ_d. P_s and $\langle P_s \rangle$ are zero exactly when $\Gamma_d = 0$ or $t_{so} = 0$. Of course, t_{so} is a key factor for the spin polarization or equivalently t_{so} is "the driving force" of P_s. If there is no SOC, no spin polarization would appear for whatever other parameters are. In general, strong SOC usually leads to large $\langle P_s \rangle$ [Fig. 4(b)]. However, for fixed E, P_s will not increase monotonically with t_{so}, as seen in Fig. 4(a). A large P_s can be obtained for long dsDNA even for quite small t_{so}, because the spin polarized electrons will accumulate gradually when the electrons are transmitting along the dsDNA. In addition, we observe a large area with red color in Fig. 4(b), where $\langle P_s \rangle$ exceeds 0.1 for short dsDNA. This implies that the dsDNA would be an efficient spin filter in a wide parameters range.

Figure 4(c) plots the averaged spin polarization $\langle P_s \rangle$ vs Γ_d and $\frac{\theta}{\pi}$ by fixing the radius R and the arc length l_a to account for the rigid sugar-phosphate backbones. The helix angle θ can be changed by stretching the DNA molecule [33]. It is obvious that $\langle P_s \rangle$ is zero in the absence of the helical symmetry ($\theta = \frac{\pi}{2}$) and is increased by decreasing θ. This indicates that the helix of the dsDNA plays a vital role to the existence of the spin polarization. Finally, we present the influence of the hopping integrals t_1 and t_2 on the spin polarization, as illustrated in Fig. 4(d). We can see that $\langle P_s \rangle$ is much bigger in a wide range of t_1 and t_2 when they have opposite sign, and the sign of $\langle P_s \rangle$ can be reversed by switching t_1 and t_2. Besides, further studies indicate that the spin polarization remains considerably large even in the presence of the disorder, e.g., the on-site energy disorder, the twist angle disorder. Accordingly, our results can also hold for other aperiodic DNA molecules.

In summary, we propose a model Hamiltonian to simulate the quantum spin transport through the dsDNA. This two-terminal dsDNA-based device would exhibit high spin polarization by considering the SOC, the dephasing, and the helical symmetry, although no spin polarization exists in the ssDNA. The spin polarization increases with increasing the DNA length. Additionally, the spin polarization could be improved by properly modifying the hopping integral and decreasing the helix angle.

This work was supported by China-973 program and NSF-China under Grants No. 10974236 and No. 10821403.

*sunqf@iphy.ac.cn

[1] A. R. Rocha, V. M. García-suárez, S. W. Bailey, C. J. Lambert, J. Ferrer, and S. Sanvito, Nature Mater. **4**, 335 (2005).
[2] A. Fert, Rev. Mod. Phys. **80**, 1517 (2008).
[3] V. A. Dediu, L. E. Hueso, I. Bergenti, and C. Taliani, Nature Mater. **8**, 707 (2009).
[4] M. Urdampilleta, S. Klyatskaya, J-P. Cleuziou, M. Ruben, and W. Wernsdorfer, Nature Mater. **10**, 502 (2011).
[5] Z. H. Xiong, D. Wu, Z. V. Vardeny, and J. Shi, Nature (London) **427**, 821 (2004).
[6] C. Barraud, P. Seneor, R. Mattana, S. Fusil, K. Bouzehouane, C. Deranlot, P. Graziosi, L. Hueso, I. Bergenti, V. Dediu, F. Petroff, and A. Fert, Nature Phys. **6**, 615 (2010).
[7] J. Brede, N. Atodiresei, S. Kuck, P. Lazić, V. Caciuc, Y. Morikawa, G. Hoffmann, S. Blügel, and R. Wiesendanger, Phys. Rev. Lett. **105**, 047204 (2010).
[8] N. Atodiresei, J. Brede, P. Lazić, V. Caciuc, G. Hoffmann, R. Wiesendanger, and S. Blügel, Phys. Rev. Lett. **105**, 066601 (2010).
[9] S. Schmaus, A. Bagrets, Y. Nahas, T. K. Yamada, A. Bork, M. Bowen, E. Beaurepaire, F. Evers, and W. Wulfhekel, Nature Nanotech. **6**, 185 (2011).
[10] F. Kuemmeth, S. Ilani, D. C. Ralph, and P. L. McEuen, Nature (London) **452**, 448 (2008).

[11] B. Göhler, V. Hamelbeck, T. Z. Markus, M. Kettner, G. F. Hanne, Z. Vager, R. Naaman, and H. Zacharias, Science **331**, 894 (2011).
[12] Z. Xie, T. Z. Markus, S. R. Cohen, Z. Vager, R. Gutierrez, and R. Naaman, Nano Lett. **11**, 4652 (2011).
[13] S. Yeganeh, M. A. Ratner, E. Medina, and V. Mujica, J. Chem. Phys. **131**, 014707 (2009).
[14] R. Gutierrez, E. Díaz, R. Naaman, and G. Cuniberti, Phys. Rev. B **85**, 081404(R) (2012).
[15] G. L. J. A. Rikken, Science **331**, 864 (2011).
[16] M. Di Ventra and Y. V. Pershin, Nature Nanotech. **6**, 198 (2011).
[17] G. Cuniberti, E. Maciá, A. Rodríguez, and R. A. Römer, in *Charge Migration in DNA: Perspectives from Physics, Chemistry and Biology*, edited by T. Chakraborty (Springer-Verlag, Berlin, 2007).
[18] D. Hochberg, G. Edwards, and T. W. Kephart, Phys. Rev. E **55**, 3765 (1997).
[19] In other words, here we consider the SOC induced by the boundary-confining potential. All the results are qualitatively same if other kinds of SOC are considered.
[20] Q.-F. Sun, X. C. Xie, and J. Wang, Phys. Rev. B **77**, 035327 (2008).
[21] X.-Q. Li and Y.-J. Yan, Appl. Phys. Lett. **79**, 2190 (2001).
[22] Y. A. Berlin, A. L. Burin, and M. A. Ratner, J. Am. Chem. Soc. **123**, 260 (2001).
[23] Y. A. Berlin, A. L. Burin, and M. A. Ratner, Chem. Phys. **275**, 61 (2002).
[24] Y. Xing, Q.-F. Sun, and J. Wang, Phys. Rev. B **77**, 115346 (2008).
[25] H. Jiang, S. Cheng, Q.-F. Sun, and X. C. Xie, Phys. Rev. Lett. **103**, 036803 (2009).
[26] Q.-F. Sun, J. Wang, and H. Guo, Phys. Rev. B **71**, 165310 (2005).
[27] *Electronic Transport in Mesoscopic Systems*, edited by S. Datta (Cambridge University Press, Cambridge, England, 1995).
[28] Y. J. Yan and H. Zhang, J. Theor. Comput. Chem. **1**, 225 (2002).
[29] R. G. Endres, D. L. Cox, and R. R. P. Singh, Rev. Mod. Phys. **76**, 195 (2004).
[30] K. Senthilkumar, F. C. Grozema, C. F. Guerra, F. M. Bickelhaupt, F. D. Lewis, Y. A. Berlin, M. A. Ratner, and L. D. A. Siebbeles, J. Am. Chem. Soc. **127**, 14894 (2005).
[31] L. G. D. Hawke, G. Kalosakas, and C. Simserides, Eur. Phys. J. E **32**, 291 (2010).
[32] Q.-F. Sun and X. C. Xie, Phys. Rev. B **71**, 155321 (2005).
[33] J. Gore, Z. Bryant, M. Nöllmann, M. U. Le, N. R. Cozzarelli, and C. Bustamante, Nature (London) **442**, 836 (2006).